Chemistry–A European Journal
Research Article
doi.org/10.1002/chem.202400766
Chemistry Europe
European Chemical Societies Publishing
www.chemeurj.org

Hot Paper

Multicationic Tetrahedra Networks: Alkaline-Earth-Centered Polyhedra and Non-Condensed AlN_6-Octahedra in the Imidonitridophosphates $AE_2AlP_8N_{15}(NH)$ (AE = Ca, Sr, Ba)

Monika M. Pointner,[a] Reinhard M. Pritzl,[a] Jonas M. Albrecht,[a] Leopold Blahusch,[a] Jonathan P. Wright,[b] Eleanor Lawrence Bright,[b] Carlotta Giacobbe,[b] Oliver Oeckler,*[c] and Wolfgang Schnick*[a]

A series of isostructural imidonitridophosphates $AE_2AlP_8N_{15}(NH)$ (AE = Ca, Sr, Ba) was synthesized at high-pressure/high-temperature conditions (1400 °C and 5–9 GPa) from alkaline-earth metal nitrides or azides Ca_3N_2/$Sr(N_3)_2$/$Ba(N_3)_2$ and the binary nitrides AlN and P_3N_5. NH_4F served as a hydrogen source and mineralizing agent. The crystal structures were determined by single-crystal X-ray diffraction and feature a three-dimensional network of vertex-sharing PN_4-tetrahedra forming diverse-sized rings that are occupied by aluminum and alkaline earth ions. These structures represent another example of nitridophosphate-based networks that simultaneously incorporate AlN_6-octahedra and alkaline-earth-centered polyhedra, with aluminum not participating in the tetrahedra network. They differ from previously reported ones by incorporating non-condensed octahedra instead of strongly condensed octahedra units and contribute to the diversity of multicationic nitridophosphate network structures. The results are supported by atomic resolution EDX mapping, solid-state NMR and FTIR measurements. Eu^{2+}-doped samples show strong luminescence with narrow emissions in the range of green to blue under UV excitation, marking another instance of Eu^{2+}-luminescence within imidonitridophosphates.

Introduction

The demand for environmentally friendly, energy-efficient, and cost-effective luminescent materials rises steadily.[1] Alkaline-earth-(*AE*)-containing nitridophosphates can offer many key characteristics crucial for phosphor-converted LED applications. One reason why they are so well suited is their diverse structural chemistry with tetrahedra-based networks and an easily changeable local environment of the alkaline-earth ions. They span the entire visible spectral range with only a handful of known compounds, and understanding the influence of structural parameters on materials properties not only allows the explanation of current characteristics but also helps to predict structure-property relationships.

Nitridophosphate networks can be characterized by their degree of condensation κ, which is defined by the atomic ratio of tetrahedra centers (P) to vertices (N) and range from non-condensed PN_4-tetrahedra ($\kappa_{min} = {}^1/_4$) to highly condensed networks with vertex- and edge-sharing tetrahedra ($\kappa_{max} = 3/5$ in P_3N_5).[2–3] Compounds with a degree of condensation $\kappa < 0.5$ exhibit structural motifs often comprising non-condensed units like non-condensed rings built up from vertex-sharing tetrahedra.[4–5] Single and double chains can differ in stretching factors and periodicity.[6–7] Structures with $0.3 \leq \kappa \leq 0.5$ can form column-type and condensed layer phosphate structures, and $\kappa > 0.5$ often results in layered structures and condensed three-dimensional networks, including a wide range of different-sized rings and channels.[8–12]

Upon doping with Eu^{2+}, three-dimensional network compounds can provide favorable properties like a small Stokes shift, low thermal quenching and high quantum efficiencies.[13] The local environment of the alkaline-earth ion and the activator ion, the symmetry, and the number of crystallographic sites may affect the number of emission maxima as well as their shape and position. High symmetry and a small number of sites are expected to result in favorable properties like a low number of emission maxima with a narrow-band emission. Different ligand atoms change the electron density between the activator ion and the ligand. Opting for oxonitridophosphates with a more red-shifted emission or incorporating halides can offer the flexibility to tune for specific emission regions.[14]

The cation ratio *CR* (ratio of counter cations to network cations) and the resulting changes in structure and physical

[a] M. M. Pointner, R. M. Pritzl, J. M. Albrecht, L. Blahusch, Prof. Dr. W. Schnick
Department of Chemistry
Ludwig-Maximilians-University Munich
Butenandtstraße 5–13, 81377 Munich, Germany
E-mail: wolfgang.schnick@uni-muenchen.de
[b] Dr. J. P. Wright, Dr. E. L. Bright, Dr. C. Giacobbe
ESRF, The European Synchrotron
71 Avenue des Martyrs, CS40220, 38043 Grenoble Cedex 9, France
[c] Prof. Dr. O. Oeckler
Institute for Inorganic Chemistry and Crystallography
Leipzig University
Scharnhorststraße 20, 04275 Leipzig, Germany
E-mail: oliver.oeckler@gmx.de

Supporting information for this article is available on the WWW under https://doi.org/10.1002/chem.202400766

properties are relatively disregarded aspects.[15] Cations that do not belong to the tetrahedra network but occupy positions that are unfavorable for activator ions are one particular research focus. These additional cations may feature their own substructures, modifying the nitridophosphate-based network. Until now, only a few such cases have been studied. The structures range from non-condensed and edge-sharing Mg-centered octahedra in $MgSrP_3N_5O_2$ and $CaMg_2P_6N_{10}O_3$ to a highly condensed vertex- and edge-sharing substructure of Al-centered octahedra as found in $SrAl_5P_4N_{10}O_2F_3$:Eu^{2+}, the first representative of multicationic nitridophosphate-based structure containing an alkaline-earth element and aluminum.[15–17]

In this context, we present the synthesis and structural characterization of the isostructural multicationic imidonitridophosphates $AE_2AlP_8N_{15}(NH)$ (AE = Ca, Sr, Ba), which contain a PN_4-tetrahedra network that gives room to AlN_6-octahedra and AE-centered polyhedra.

Results and Discussion

Synthesis: Eu^{2+}-doped and undoped representatives of the imidonitridophosphates $AE_2AlP_8N_{15}(NH)$ (AE = Ca, Sr, Ba) were obtained by applying high-pressure high-temperature conditions (T = 1400 °C, p = 5 GPa for Sr and Ba, 9 GPa for Ca). The syntheses are assumed to follow the reaction equations (1) and (2). $AE(N_3)_2$ (AE = Sr, Ba) or Ca_3N_2, α-P_3N_5, AlN and NH_4F were used as starting materials (Table S1). EuF_3 was used as an europium source, and NH_4F functions as a hydrogen source as well as a mineralizing agent. Further details of the multianvil setup are given in the Experimental Section.

$$6\ AE(N_3)_2 + 8\ P_3N_5 + 3\ AlN + NH_4F \rightarrow 3\ AE_2AlP_8N_{15}(NH) + 16\ N_2 + HF \quad (1)$$

.

$$2\ Ca_3N_2 + 8\ P_3N_5 + 3\ AlN + NH_4F \rightarrow 3\ Ca_2AlP_8N_{15}(N + HF \quad (2)$$

The title compounds are yielded as crystalline solids with a light-gray body color. They are stable towards air and moisture, and samples doped with Eu^{2+} show photoluminescence in the range of green to blue upon irradiation with UV light. Crystallites exhibit a rod-shaped morphology with lengths of up to 100 μm and widths of around 50 μm for $Ca_2AlP_8N_{15}(NH)$ and $Ba_2AlP_8N_{15}(NH)$ (Figure 1). Synthesis for $Sr_2AlP_8N_{15}(NH)$ yielded microcrystalline material.

Crystal Structure Determination: The crystal structures of $AE_2AlP_8N_{15}(NH)$ (AE = Ca, Sr, Ba) were solved and refined from single-crystal X-ray diffraction (SCXRD) data in the orthorhombic space group *Pnma* (no. 62). Table 1 summarizes the details of the structure determinations. Wyckoff positions, atomic coordinates and displacement parameters are given in the Supporting Information (Tables S2–S7). A tilt series of selected area electron diffraction (SAED) patterns matches simulations and confirms unit cell metrics (Figure S1). Pre-characterization of

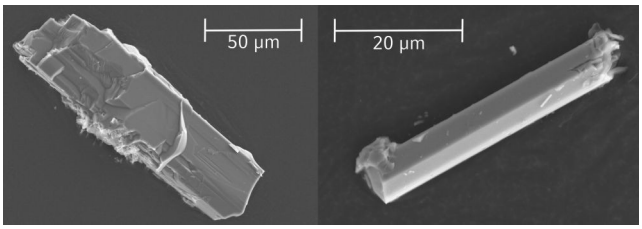

Figure 1. Secondary electron image of $Ca_2AlP_8N_{15}(NH)$:Eu^{2+} (left) and $Ba_2AlP_8N_{15}(NH)$:Eu^{2+} (right).

crystallites by transmission electron microscopy (TEM) made it possible to obtain single-crystal data of $Sr_2AlP_8N_{15}(NH)$ (Figure S2). Crystals of around 2–3 μm in size were identified on TEM grids by energy dispersive X-ray (EDX) spectroscopy and SAED patterns, and SCXRD data were collected with micro-focused synchrotron radiation at the beamline ID11 of the ESRF (Grenoble, France).

Rietveld refinements on powder X-ray diffraction (PXRD) data were used to analyze the phase compositions. No crystalline side phases are present for samples of $AE_2AlP_8N_{15}(NH)$ (AE = Sr, Ba), and $Ca_2AlP_8N_{15}(NH)$ is the main phase next to CaP_8N_{14} (Figures 2 and S3–S4). High-temperature PXRD on $Ba_2AlP_8N_{15}(NH)$ demonstrates stability up to at least 900 °C in air and shows only very little change in lattice parameters or cell volume (Figure S5).

Lattice energy (MAPLE), bond valence sum (BVS) and charge distribution (CHARDI) calculations support the structure model (Tables S8–S11). They show the lowest "charge" for the N1 and N7 sites, indicating either hydrogen in their vicinity or a positional disorder of nitrogen and oxygen. The elemental compositions were analyzed by EDX spectroscopy (Table S12), and crystals exemplarily used for electron microscopy analysis are shown in Figure S6. Some EDX measurements show a significant oxygen peak, few cases even exceeding expected values of a possible N/O disorder, which could indicate a sensitivity to moisture. Slight compositional variations cannot be ruled out, and a phase width according to $AE_2AlP_8N_{15}(NH)_xO_{1-x}$ (x = 0–1) could be considered. However,

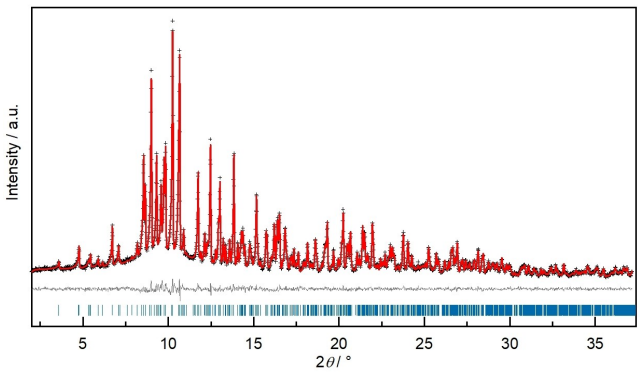

Figure 2. Rietveld refinement for $Ba_2AlP_8N_{15}(NH)$:Eu^{2+}; observed (black data points) and calculated (red line) PXRD patterns, positions of Bragg reflections of $Ba_2AlP_8N_{15}(NH)$:Eu^{2+} (vertical blue bars), and difference profile (gray line); R_p = 0.035, R_{wp} = 0.048, R_{exp} = 0.016, R_{Bragg} = 0.019.

Table 1. Crystallographic data of $AE_2AlP_8N_{15}(NH):Eu^{2+}$ (AE = Ca, Ba) and $Sr_2AlP_8N_{15}(NH)$.

formula	$Ca_{1.89}Eu_{0.11}AlP_8N_{15}(NH)$	$Sr_2AlP_8N_{15}(NH)$	$Ba_{1.89}Eu_{0.11}AlP_8N_{15}(NH)$
molar mass/g·mol^{-1}	592.85	675.13	776.21
crystal system		orthorhombic	
space group		*Pnma* (no. 62)	
lattice parameters/Å	a = 13.1482(4) b = 8.0446(3) c = 11.4981(4)	a = 13.261(3) b = 8.0610(16) c = 11.636(2)	a = 13.5546(2) b = 8.16370(10) c = 11.8541(2)
cell volume/Å^3	1216.18(7)	1243.9(4)	1311.72(3)
formula units/unit cell		4	
density/g·cm^{-3}	3.238	3.605	3.930
temperature/K	297(2)	293(2)	297(2)
absorption correction		semiempirical	
radiation	Mo-Kα (λ = 0.71073 Å)	synchrotron (λ = 0.2882 Å)	**Mo-Kα (λ = 0.71073 Å)**
μ/mm^{-1}	2.636	0.874	7.248
F(000)	1163.7	1288	1435.2
d_{min}/Å	0.6500	0.7000	0.6000
total no. of reflections	37804	18636	78015
independent reflections [$I \geq 2\sigma(I)$/all]	2347/2429	1813/2001	**3082/3345**
R_σ, R_{int}	0.0125, 0.0284	0.0342, 0.0623	0.0163, 0.0469
refined parameters	141	137	139
restraints		1	
GooF	1.343	1.079	1.117
R values [$I \geq 2\sigma(I)$]	$R1$ = 0.0263, $wR2$ = 0.0619	$R1$ = 0.0242, $wR2$ = 0.0584	$R1$ = 0.0151, $wR2$ = 0.0343
R values (all data)	$R1$ = 0.0273, $wR2$ = 0.0622	$R1$ = 0.0273, $wR2$ = 0.0596	$R1$ = 0.0177, $wR2$ = 0.0348
$\Delta\rho_{max}$, $\Delta\rho_{min}$/e·Å^{-3}	0.683, −0.563	0.965, −0.734	1.147, −1.002

magic angle spinning (MAS) NMR data show a clear signal in the ^1H and in the cross-polarized $^1H \rightarrow ^{31}P$ spectra, which are discussed in detail in the NMR section. FTIR data of Sr and Ba compounds show weak but present absorption bands in the region of N–H stretching vibrations (Figure S7), suggesting imide groups.[18] The position of H for all structures was determined from difference Fourier maps. The N1–H1 bond length was restrained at 0.90 Å, and the thermal displacement parameter of H1 was refined together with N1.

Structure Description: The structures consist of a three-dimensional network of vertex-sharing PN_4-tetrahedra incorporating channels occupied by Al^{3+} and AE^{2+} (AE = Ca, Sr, Ba) ions (Figure 3). The channels are created by six- and twelve-membered rings interconnected along *b*. The topology of the anionic network is described by the point symbol {3.4.5.6^2.7}2{3.6^5}{6^6} as calculated using TOPOS.[19] The mineral paracelsian $BaAl_2Si_2O_8$ (Figure S8) shows a similar structure with smaller four- and eight-membered rings, but this exact topology has not been found for tetrahedra networks so far.[20]

The anionic network is built up by four crystallographically distinct vertex-sharing PN_4-tetrahedra. Interatomic P–N distances and N–P–N angles vary between 1.592(2)–1.6627(16) Å and 98.99(11)–118.99(6)°, which is in good agreement with known nitridophosphates.[15–17] Bond lengths and bonding angles of the network do not change significantly when the polyhedra of the AEN_x-polyhedra (x = 8–10) increase in size from Ca to Ba.

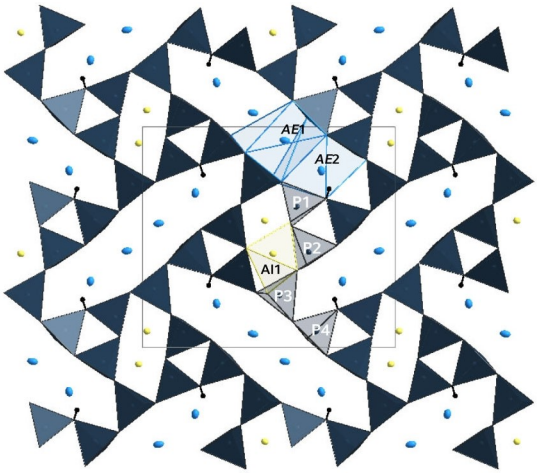

Figure 3. Projection of the crystal structure of $Ba_2AlP_8N_{15}(NH)$ along [010]. Ba bright blue, Al yellow and $PN_4/PN_3(NH)$-tetrahedra dark blue with H black. Cationic sites are partially labeled. Gray lines highlight the unit cell. The atoms are displayed with anisotropic displacement ellipsoids at 90% probability.

Figure 4 depicts all coordination polyhedra. An overview of interatomic distances and angles is provided in Tables S12–S15. The tetrahedra network contains rings condensed to channels running along *b*. These channels can be separated into void channels formed by rings of three vertex-sharing tetrahedra,

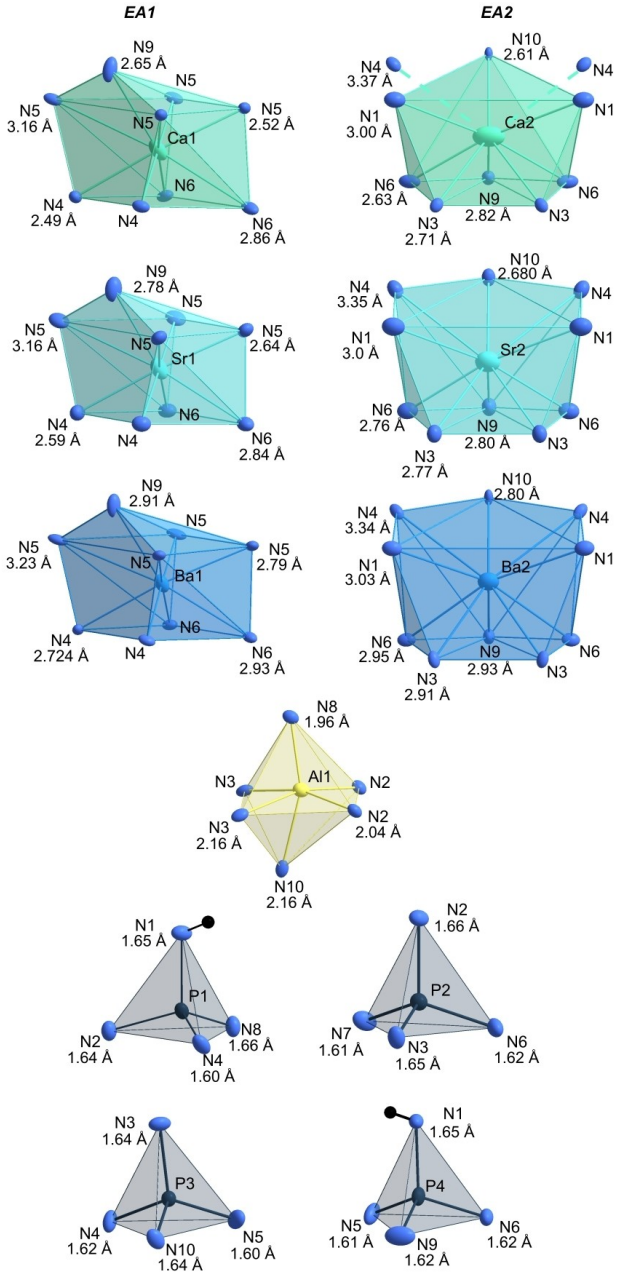

Figure 4. Coordination polyhedra around *AE*1, *AE*2 (*AE* = Ca, Sr, Ba), Al1 and P1–P4. Atoms are displayed with anisotropic displacement ellipsoids at 90% probability; coordination spheres of *AE*1 (CN = 9) and *AE*2 (CN = 8 for Ca and 10 for Sr, Ba). Polyhedra and interatomic distances for Al1 and P1–P4 are given for $Ba_2AlP_8N_{15}$(NH). All interatomic distances with standard deviations are given in the Tables S10–S12.

channels formed by rings of six vertex-sharing tetrahedra occupied by Al^{3+} and channels formed by rings of twelve vertex-sharing tetrahedra occupied by AE^{2+}. These rings are interconnected along *b* by up- and downward pointing tetrahedra. Figure S9 illustrates the different ring types and shows the additional rings along the columns. In the case of the six-membered rings, these are additional six-membered rings, and in the case of twelve-membered rings, additional four- and six-membered rings.

Alkaline-earth atoms occupy channels formed by condensed twelve-membered rings. Eight to ten nitrogen atoms coordinate two distinct crystallographic positions. The *AE*-centered polyhedra share vertices and edges. Interatomic *AE*–N distances are in agreement with the literature and slightly increase from 2.4933(16)–3.1545(17) Å for Ca, over 2.5894(19)–3.3476(19) Å for Sr to 2.7240(11)–3.3354(12) Å for Ba.[7, 10, 13] The *AE*1 site is coordinated by nine nitrogen atoms, and the resulting polyhedron can be described as a monocapped distorted tetragonal prism. In the case of Ba and Sr, the *AE*2 site is coordinated by ten nitrogen atoms, and the resulting polyhedron can described as a distorted pentagonal prism. For the Ca2 site, partial BVS values indicate that only eight nitrogen atoms, instead of ten, contribute to strong bonds (Table S9), resulting in 8-fold coordination and a dicapped distorted pentagonal prism. This coincides with, e.g., $BaCa_2P_6N_{12}$, in which Ca is 9-fold coordinated, and Ba is 12-fold coordinated.[21]

Aluminum atoms occupy the smaller channels formed by six-membered rings. The resulting AlN_6-octahedra are not connected to each other but share edges and vertices with PN_4-tetrahedra (Figure S10). Al^{3+} ions are slightly displaced from the center of the octahedra, which results in Al–N8 being the shortest and Al–N10 the longest bond lengths. Interatomic Al–N distances range between 1.948(2)–2.151(2) Å (Ca), 1.936(3)–2.136(3) Å (Sr) and 1.9565(17)–2.1658(17) Å (Ba). As the size of the alkaline-earth polyhedra increases, the octahedra slightly increase in volume due to the expansion of the network.

The structure model has been validated by scanning transmission electron microscopy high-angle annular dark-field (STEM-HAADF) images with a *Z*-contrast according to Z^2.[22] The established structure agrees well with STEM-HAADF images obtained along the zone axes [010] and [101] (Figure 5 upper parts). The projection along [010] shows distinct intensities for the alkaline-earth ions, and the positions of all phosphorus ions are resolved. Aluminum is not visible due to its low atomic fraction, the large *Z* contrast between Ba ($Z = 56$) and Al ($Z = 13$), and the low number of atoms within the Al columns. However, STEM-EDX maps along the same projection reveal aluminum in the anticipated positions (Figure 5 lower parts). Regions rich in respective elements are clearly separated from others in both directions, and a possible disorder of Al and P atoms on either octahedral or tetrahedral positions can be ruled out. Enlarged versions and raw EDX spectra are given in the Figures S12–S15.

Solid-state NMR: ^{27}Al, ^{1}H, ^{31}P and cross-polarized $^{1}H \rightarrow ^{31}P$ MAS NMR spectra of $Ba_2AlP_8N_{15}$(NH) and ^{1}H MAS NMR spectra of $Sr_2AlP_8N_{15}$(NH) were measured (Figure 6). The resonance line of the central transition in the ^{27}Al (spin $I = 5/2$) NMR spectrum shows one Al signal centered around $\delta = 5.4$ ppm (Figure 6a). A narrow signal indicates a highly symmetrical position with low quadrupolar interaction, and the shift is in the range of octahedrally N-coordinated Al reported in the literature.[11, 23] Each of the solid-state ^{1}H NMR spectra (Figure 6b) features a peak attributable to the imide group ($\delta = 6.5$ ppm), agreeing with literature values.[24] The additional signal at $\delta = 7.5$ ppm could be attributed to NH_4^+, presumably from an unknown

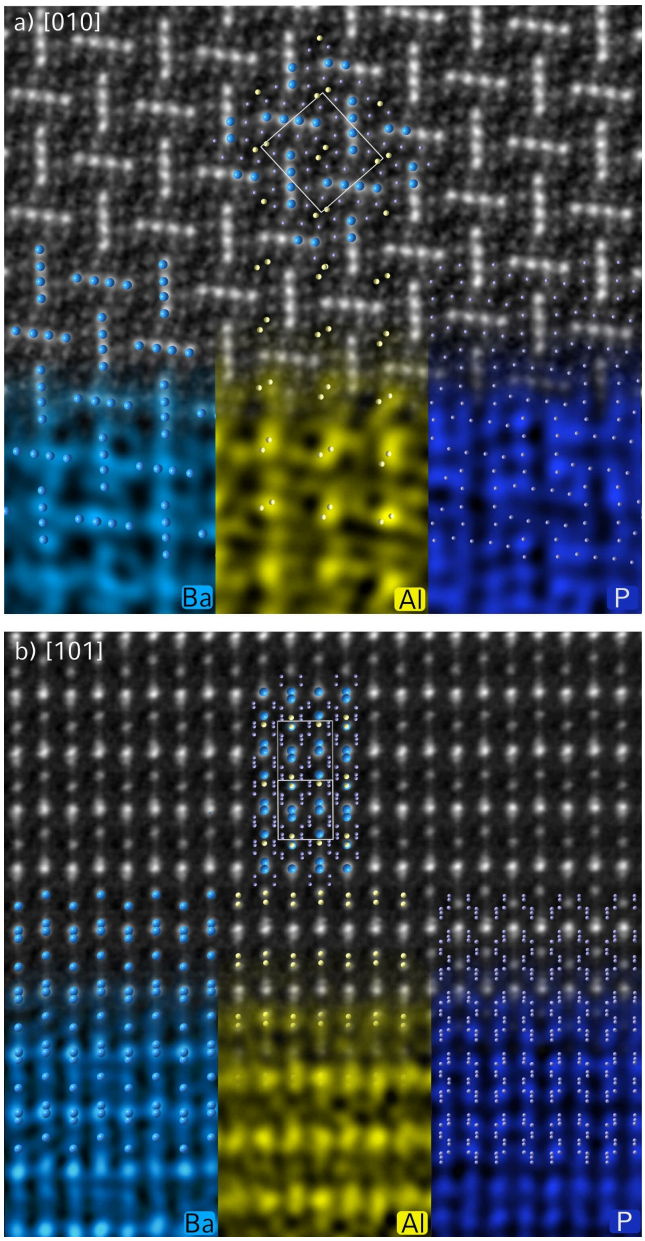

Figure 5. STEM-EDX maps of $Ba_2AlP_8N_{15}$(NH) along **a**) [010] and **b**) [010]; STEM-HAADF image (top) with structure overlay (middle, Ba bright blue, Al yellow, P pale blue) and corresponding EDX maps (bottom); the unit cell is shown in the insert in light gray. Enlarged versions are shown in the Supporting Information.

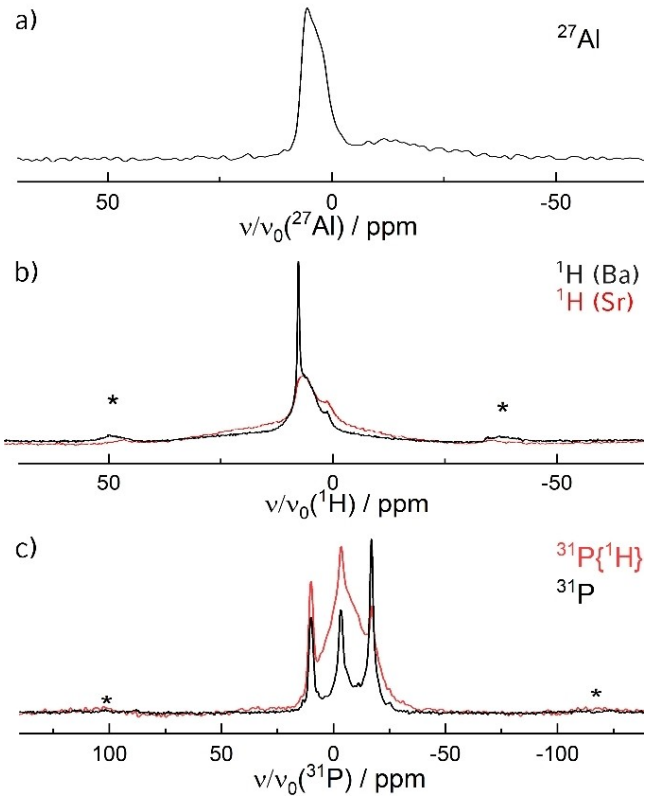

Figure 6. Solid-state MAS NMR spectra of $Ba_2AlP_8N_{15}$(NH); **a**) One signal in the ^{27}Al spectrum (10 kHz); **b**) ^{1}H spectra (both 20 kHz) of $Ba_2AlP_8N_{15}$(NH) (black) and $Sr_2AlP_8N_{15}$(NH) (red), two signals appear in both measurements and one high-intensity signal only appears in the $Ba_2AlP_8N_{15}$(NH) spectrum; latter may originate in a NH_4^+ containing side phase; **c**) Three signals in the ^{31}P spectrum (black) with an estimated integral ratio 1:1:2 and three overlapping signals in the ^{1}H→^{31}P spectrum (both 20 kHz), showing a coupling of H to at least three P sites; sidebands are marked with asterisks.

secondary phase.[24] It could not be unambiguously clarified whether the signal at $\delta = 1.2$ ppm in both measurements originates from the target compound or an unknown secondary phase. The ^{31}P spectrum shows three signals at $\delta = 9.88$, -3.42 and -17.11 ppm with an estimated integral ratio of 1:1:2 (Figure 6c). This is in the typical range for tetrahedrally N-coordinated P, as observed in, e.g., AlP_6N_{11} and $AlP_6O_{3x}(NH)_{3-x}N_9$.[11,25] The intensity distribution is consistent with four crystallographically independent P sites when two P sites have a similar chemical environment. This leads to a signal overlap at -17.11 ppm with a roughly doubled intensity. To confirm the proximity of H to the P atoms, magnetization was transferred from ^{1}H to ^{31}P. The presence of three signals in cross-polarized experiments with $\delta = 9.9$, -3.5, -17.3 ppm indicates the vicinity of H to at least three P atom sites. They align with the phosphorus signals present in the ^{31}P measurement. This supports the assumption of an imido group in the structure and the localization of H bound to N1, as this position enables spatial proximity to all P sites.

Luminescence: Eu^{2+}-doped samples of $AE_2AlP_8N_{15}$(NH) (AE = Ca, Sr, Ba) (~5 mol% Eu^{2+} with respect to the AE content) can be excited by near-UV to blue light, showing strong luminescence with narrow emissions in the visible spectral region (Figure 7, unsmoothed spectra Figure S16). The emission curve of $Ca_2AlP_8N_{15}$(NH):Eu^{2+} was extrapolated using Savitzky-Golay-Filter to enable a comparison of the emission spectra. Excitation at 400 nm (AE = Ba, Sr) and 450 nm (AE = Ca) results in blue to green luminescence and one emission band for all compounds ($Ca_2AlP_8N_{15}$(NH):Eu^{2+}: $\lambda_{max} = 512$ nm, $fwhm = 54$ nm/2018 cm^{-1}; $Sr_2AlP_8N_{15}$(NH):Eu^{2+}: $\lambda_{max} = 496$ nm, $fwhm = 46$ nm/1859 cm^{-1}; $Ba_2AlP_8N_{15}$(NH):Eu^{2+}: $\lambda_{max} = 474$ nm, $fwhm = 38$ nm/1666 cm^{-1}). Based on the ionic radius of Eu^{2+}, only the AE sites are considered because the octahedrally coordinated Al^{3+} site and the tetrahedrally coordinated P^{5+} sites are not suitable for Eu^{2+}

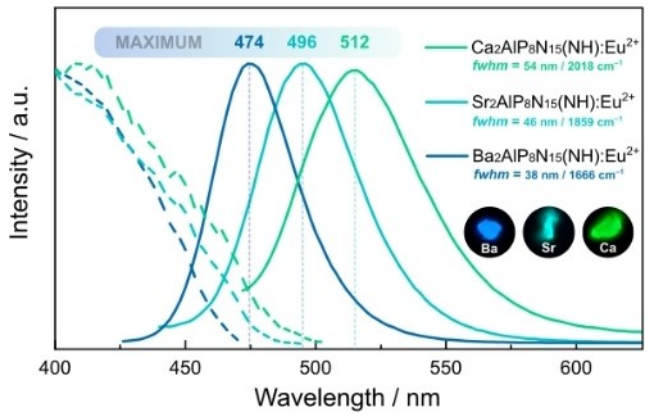

Figure 7. Single particle luminescence spectra of $AE_2AlP_8N_{15}(NH):Eu^{2+}$ (AE = Ca, Sr, Ba). Normalized excitation spectra (left) (Ca λ_{exc} = 450 nm, Sr/Ba λ_{exc} = 400 nm) and emission spectra (middle) for Ca (green), Sr (cyan), Ba (blue); insert: photograph of luminescent particles (λ_{exc} = 420 nm).

due to their much smaller size (ionic radii P^{5+}: 17 pm, Al^{3+}: 53.5 pm, Ca^{2+}: 112–123 pm, Sr^{2+}: 131–136 pm, Ba^{2+}: 147–152 pm, Eu^{2+}: 125–135 pm).[26] In general, the luminescence of Eu^{2+}-doped compounds strongly depends on the immediate environment of the activator site. The luminescence series of the three compounds shows a strong dependence on AE^{2+}–N distances. An excitation of $Ca_2AlP_8N_{15}(NH):Eu^{2+}$ at 420 nm shows a smaller second band with a maximum at 455 nm (Figure S17). Due to the high chemical similarity of the two Ca sites (polyhedral volume Ca1 ≈ 35.4 Å^3, Ca2 ≈ 31.7 Å^3), we assume both sites were doped. Comparing the distances between the nearest ligands of the two Ca sites, the N atoms coordinate closer to Ca1 than to Ca2 (d_{Ca1-N4}: 2.493(2) Å, $d_{Ca2-N10}$: 2.608(2) Å) and the average Ca–N distances are shorter for Ca1 ($d_{ø}$Ca1–N: 2.744 Å, $d_{ø}$Ca2–N: 2.762 Å). Shorter distances result in an increase in the nephelauxetic effect, and the red-shifted band with a maximum at λ_{max} = 516 nm is likely caused by doping of the Ca1 site, whereas the second band with a maximum at around 455 nm should result from doping of the Ca2 site. The observation of the second band can help to explain the observed luminescence of the other two compounds. The observed emission bands of $AE_2AlP_8N_{15}(NH):Eu^{2+}$ (AE = Sr, Ba) could originate from doping of the AE1 site, as well, whereas possible further emission bands lie within the UV range and cannot be detected with the measurement setup used. This is consistent with the narrow band emission of $Ba_2AlP_8N_{15}(NH):Eu^{2+}$, compared to similar Ba compounds, which contain only one Ba site as well, such as $BaP_8N_{14}:Eu^{2+}$, $BaP_6N_{11}NH:Eu^{2+}$ (λ_{em} = 417/460 nm, *fwhm* = 2075/2423 cm^{-1}).[10,27] Due to the very similar ionic radii of Sr^{2+} and Eu^{2+} (Sr^{2+}: 131–136 pm, Eu^{2+}: 125–135 pm), it is possible that the emission maximum nevertheless originates from doping of both sites, but our results agree with findings in the literature, which describe that Eu^{2+} preferentially occupies sites < 40 Å^3 (Sr1 ≈ 37.8 Å^3, Sr2 ≈ 43.2 Å^3).[28] Theoretical spectroscopy studies could be made to verify these results further.[29]

Conclusions

The isostructural compounds $AE_2AlP_8N_{15}(NH)$ with AE = Ca, Sr, Ba were obtained by NH_4F-mediated HP/HT syntheses. Their crystal structures were determined by single-crystal X-ray diffraction. Electron microscopy, EDX mapping with atomic resolution, and solid-state NMR studies agree with the structure model. The non-condensed Al-centered octahedra represent a structural motif that differs strongly from other nitridophosphate-based compounds, e.g., $SrAl_5P_4N_{10}O_2F_3$, which forms a highly condensed substructure of edge-sharing Al-centered octahedra. The compounds show emission from blue to green upon doping with Eu^{2+} and belong to the small group of imidonitridophosphates exhibiting luminescent properties. We expect that research on further modifying the nitridophosphate network with additional cations not participating in the tetrahedra network, e.g., Mg^{2+} ions, opens up the possibility to access a number of stable compounds with diverse structural motifs featuring interesting luminescent properties. Plus, a possible site-selectivity of doping due to differences in charge and ionic radii of Al^{3+} and AE^{2+} makes it possible to modify the luminescence not only by metal-ligand distances or coordination geometry but also by choice of the emitter (e.g., Cr^{3+} on Al^{3+} sites versus Eu^{2+} on AE^{2+} sites).[30] This makes research on multicationic phosphors, especially aluminum-containing nitrides and nitridophosphates, a promising field worth investigating.

Experimental Section

Preparation of starting materials: Alkaline-earth element azides $AE(N_3)_2$ (AE = Sr, Ba) were prepared by reaction of the respective alkaline-earth element carbonates ($SrCO_3$: Sigma Aldrich, 99.995 %; $BaCO_3$: Grüssing, 99.8 %) with in situ generated aqueous HN_3.[31] A solution of HN_3 is formed by passing an aqueous solution of NaN_3 (Acros Organics, 99 %, extra pure) through a cation exchanger (Amberlyst 15). Formed HN_3 dropped into a suspension of the carbonate in water until the eluate showed a neutral pH value. Carbonate residues were filtered off, and the solvent was removed with a rotary evaporator (50 mbar, 40 °C). The products were obtained as colorless powders, recrystallized from acetone, and dried under vacuum. PXRD and FTIR spectroscopy confirmed the purity. Partially crystalline P_3N_5 was prepared following the synthesis of Stock et al..[32] A fused silica tube and silica boat were dried at 1273 K under dynamic vacuum (< 10^{-3} bar), and P_4S_{10} (Sigma-Aldrich, 99.99 %) was loaded in a constant flow of argon. The setup was flooded with dry ammonia (Air Liquide, 5.0) for 4 h. The reaction was carried out at 1123 K for 4 h before the furnace was cooled to room temperature with heating and cooling ramps of 5 K/min. The product was washed with diluted HCl and H_2O and yielded as an orange powder. PXRD and CHNS analysis confirmed its purity (C 0 %, H 0 %, N 42.69 %, S 0 %; expected C 0 %, H 0 %, N 42.98 %, S 0 %). Ca_3N_2 (Sigma Aldrich, 99.5 %), AlN (abcr, grade B) and EuF_3 (Sigma Aldrich, 99.99 %) were used as purchased.

Multianvil synthesis: Eu-doped and undoped $AE_2AlP_8N_{15}(NH)$ (AE = Ca, Sr, Ba) were synthesized under high-pressure high-temperature conditions with T = 1400 °C, p = 5 GPa for Sr, Ba, and T = 1400 °C, p = 9 GPa for Ca using a 1000 t hydraulic press (Voggenreiter, Mainleus, Germany) with a modified Walker module. Details on the preparation and handling of the 1000 t Walker-type multianvil press

are described in the literature.[33–36] The starting materials Ca_3N_2/$Sr(N_3)_2$/$Ba(N_3)_2$, AlN, P_3N_5, NH_4F, and if needed, EuF_3 as a doping agent (Table S1) were thoroughly ground in an agate mortar in an Ar-filled glovebox (Unilab, MBraun, Garching, $O_2 < 1$ ppm, $H_2O <$ 0.1 ppm), transferred into a crucible of h-BN (HeBoSint® S100, Henze, Kempten, Germany) and sealed with a h-BN lid. For Sr- and Ba-containing samples: After sample insertion, the setup was compressed to 5 GPa and heated to 1400 °C within 60 minutes. The temperature was held constant for 300 minutes before cooling to room temperature and slow decompression within 60 minutes. For Ca-containing samples: The setup was compressed to 9 GPa and heated to 1400 °C within 30 minutes. The temperature was held constant for 150 minutes before cooling and decompression within 30 minutes.

Powder X-ray diffraction (PXRD): A powder diffractometer Stadi P (Stoe & Cie GmbH, Germany) with either a Cu- or Ag-Kα_1 radiation ($\lambda = 1.54056$ Å and 0.5595378 Å; Ge(111) single-crystal monochromator) with modified (parafocusing) Debye-Scherrer geometry and a MYTHEN 1 K Si strip detector (Dectris Ltd., Baden, Switzerland) was used. Samples were finely ground and transferred into glass capillaries (Ø 0.3 mm, wall thickness 0.01 mm, Hilgenberg GmbH, Malsfeld, Germany). Powder diffraction patterns of $Ba_2AlP_8N_{15}(NH)$ were recorded with Ag-Kα_1 radiation at an angular range of $2\theta = 3$–37° and a step width of 0.015°. Powder diffraction patterns of $Ca_2AlP_8N_{15}(NH)$ and $Sr_2AlP_8N_{15}(NH)$ were recorded with Cu-Kα_1 radiation at an angular range of $2\theta = 3$–92° with a step width of 0.015°. TOPAS Academic 6.1 was used for Rietveld refinements, employing a fundamental parameter approach and a Chebyshev polynomial for background modeling.[37–38]

Temperature-dependent powder X-ray diffraction was carried out on a STOE StadiP diffractometer equipped with a high-temperature graphite furnace, an image plate position sensitive detector, Ag-Kα_1 radiation ($\lambda = 0.5595378$ Å) and a Ge(111) monochromator. Powder diffraction patterns were collected up to 900 °C with 50 °C increments.

Scanning electron microscopy (SEM): Isolated crystals of the compounds were placed on a conducting carbon foil and coated with carbon. Secondary electron images were obtained with a FEI Helios NanoLab G3 DualBeam UC (FEI, USA).

Scanning transmission electron microscopy (STEM): Samples were ground thoroughly in absolute ethanol and distributed on Cu grids covered with lacey carbon film (S-166-2, Plano GmbH, Germany). The grids were mounted in an analytical double-tilt holder (tilt ranges ±30°) and analysis was carried out with a Titan Themis 300 (FEI, USA) transmission electron microscope equipped with a Schottky type high-brightness electron gun (X-FEG), a post-column filter (Enfinium ER-799, Gatan, USA), a spherical aberration (Cs) corrector (DCOR, CEOS, Germany), a camera system (US 1000XP, Gatan, Germany), a 4k×4k FEI Ceta CMOS camera (FEI, USA) and a windowless 4-quadrant Super-X energy-dispersive X-ray spectroscopy detector. The system was operated at an acceleration voltage of 300 kV. Data processing and Fourier filtering were performed using Digital Micrograph (Fourier filtering), ProcessDiffraction7 (calculations of SAED patterns), jEMS (SAED simulations) and Velox (STEM images, EDX maps).[39–42]

Single-crystal X-ray diffraction (SCXRD): A Bruker D8 Venture TXS diffractometer (rotating anode, Mo-Kα radiation, $\lambda = 0.71073$ Å, multilayer monochromator) was used to obtain single-crystal X-ray diffraction data of $Ba_2AlP_8N_{15}(NH):Eu^{2+}$ and $Ca_2AlP_8N_{15}(NH):Eu^{2+}$. For indexing, integration and semiempirical absorption correction, the program package APEX3 was used.[43]

Single-crystal diffraction data with synchrotron radiation were collected for $Sr_2AlP_8N_{15}(NH)$ at beamline ID11 (ESRF, France) at ambient conditions. Crystallites on TEM finder grids (S-160, Plano GmbH, Germany) were optically centered in the synchrotron beam ($\lambda = 0.28820$ Å) with a high-magnification telescope. Centering was optimized by fluorescence and diffraction scans utilizing a hexapod setup (Symétrie Hexapods Nanopos and PI-MARS P561 piezo stage). Data were collected using a Dectris Eiger2 X 4 M CdTe detector. Indexing and integration were performed with the CrysAlis^{Pro} software package.[44] Semi-empirical absorption correction was done with SADABS.[45]

The structure solution was performed using direct methods (SHELXS) and refined against F^2 using full-matrix least-squares methods (SHELXL-2018).[46] Crystal structures were visualized using Diamond3.[47]

Bond valence sum (BVS) and CHARDI calculations: VaList was used to perform BVS calculations.[48–49] Vesta was used to perform CHARDI calculations.[50]

Madelung Part of Lattice Energy (MAPLE): The program MAPLE (Madelung part of lattice energy) was used to verify the assignment of nitrogen (vs. oxygen).[51–52]

Solid-state magic-angle spinning (MAS) NMR spectroscopy: An Advance III 500 (Bruker, Karlsruhe) equipped with an 11.7 T magnet operating at 500.25 MHz ^{1}H frequency, and a commercial double resonance MAS probe was used to record solid-state MAS NMR spectra. The sample was ground and packed into a ZrO_2 rotor with an outer diameter of 2.5 mm. At 20 kHz spinning frequency, ^{1}H, ^{31}P and ^{1}H→^{31}P spectra were recorded. The ^{27}Al spectrum was recorded at 10 kHz spinning frequency.

FTIR spectroscopy: FTIR spectra in attenuated total reflection mode were recorded on a Spectrum BX II spectrometer (PerkinElmer, MA, USA) with a DuraSampler ATR unit. Data of the title compounds were obtained in the range of 650–4400 cm^{-1}.

Luminescence measurements: Luminescence measurements of Eu^{2+}-doped $AE_2AlP_8N_{15}(NH)$ samples with AE = Ca, Sr, Ba were carried out on small particles in air. The spectra were obtained on a HORIBA Fluoromax4 spectrofluorimeter system, attached via optical fibers to an Olympus BX51 microscope. $Ca_2AlP_8N_{15}(NH):Eu^{2+}$ was measured with $\lambda_{exc} = 420$ and 450 nm, $Sr_2AlP_8N_{15}(NH):Eu^{2+}$ and $Ba_2AlP_8N_{15}(NH):Eu^{2+}$ with $\lambda_{exc} = 400$ nm. Emission spectra were recorded at room temperature with a step size of 2 nm and ranged from 400 to 800 nm.

Supporting Information

Deposition Numbers 2301149–2301151 contain the supplementary crystallographic data for this paper. These data are provided free of charge by the joint Cambridge Crystallographic Data Centre and Fachinformationszentrum Karlsruhe Access Structures service www.ccdc.cam.ac.uk/structures.

The data that support the findings of this study are available in the Supporting Information of this article. The authors have cited additional references within the Supporting Information.[53–60]

Acknowledgements

Financial support by the Deutsche Forschungsgemeinschaft (projects SCHN377/18-1 and OE530/6-1) is gratefully acknowl-

edged. The authors thank Dr. Peter Mayer and Christian Minke for single-crystal data collection, MAS NMR and SEM measurements, Jennifer Steinadler (all Department of Chemistry, LMU Munich) for the helpful discussions of the resulting NMR spectra, as well as Dr. P. Strobel and Dr. P. J. Schmidt (Lumileds Phosphor Center, Aachen) for luminescence measurements. We acknowledge beamtime at the ESRF for the acquisition of microfocused single-crystal diffraction data (project CH-5663). Open Access funding enabled and organized by Projekt DEAL.

Conflict of Interests

The authors declare no conflict of interest.

Data Availability Statement

The data that support the findings of this study are available in the supplementary material of this article.

Keywords: aluminum · electron microscopy · high-pressure chemistry · nitrides · nitridophosphates

[1] H. A. Höppe, *Angew. Chem.* **2009**, *121*, 3626–3636; *Angew. Chem. Int. Ed.* **2009**, *48*, 3572–3582.
[2] A. Marchuk, P. Schultz, C. Hoch, O. Oeckler, W. Schnick, *Inorg. Chem.* **2016**, *55*, 974–982.
[3] S. Horstmann, E. Irran, W. Schnick, *Angew. Chem.* **1997**, *109*, 1938–1940; *Angew. Chem. Int. Ed.* **1997**, *36*, 1873–1875.
[4] E. M. Bertschler, R. Niklaus, W. Schnick, *Chem. Eur. J.* **2017**, *23*, 9592–9599.
[5] J. Liu, P. S. Whitfield, M. R. Saccomanno, S.-H. Bo, E. Hu, X. Yu, J. Bai, C. P. Grey, X.-Q. Yang, P. G. Khalifah, *J. Am. Chem. Soc.* **2017**, *139*, 9192–9202.
[6] V. Schultz-Coulon, W. Schnick, *Z. Anorg. Allg. Chem.* **1997**, *623*, 69–74.
[7] M. Mallmann, S. Wendl, P. Strobel, P. J. Schmidt, W. Schnick, *Chem. Eur. J.* **2020**, *26*, 6257–6263.
[8] E. Mugnaioli, S. J. Sedlmaier, O. Oeckler, U. Kolb, W. Schnick, *Eur. J. Inorg. Chem.* **2012**, *121*, 121–125.
[9] S. J. Sedlmaier, E. Mugnaioli, O. Oeckler, U. Kolb, W. Schnick, *Chem. Eur. J.* **2011**, *17*, 11258–11265.
[10] S. Wendl, L. Eisenburger, P. Strobel, D. Günther, J. P. Wright, P. J. Schmidt, O. Oeckler, W. Schnick, *Chem. Eur. J.* **2020**, *26*, 7292–7298.
[11] S. J. Ambach, M. M. Pointner, S. Falkai, C. Paulmann, O. Oeckler, W. Schnick, *Angew. Chem.* **2023**, e202303580; *Angew. Chem. Int. Ed.* **2023**, e202303580.
[12] S. D. Kloß, L. Neudert, M. Döblinger, M. Nentwig, O. Oeckler, W. Schnick, *J. Am. Chem. Soc.* **2017**, *139*, 12724–12735.
[13] A. Marchuk, S. Wendl, N. Imamovic, F. Tambornino, D. Wiechert, P. J. Schmidt, W. Schnick, *Chem. Mater.* **2015**, *27*, 6432–6441.
[14] A. Marchuk, W. Schnick, *Angew. Chem.* **2015**, *127*, 2413–2417; *Angew. Chem. Int. Ed.* **2015**, *54*, 2383–2387.
[15] R. M. Pritzl, N. Prinz, P. Strobel, P. J. Schmidt, D. Johrendt, W. Schnick, *Chem. Eur. J.* **2023**, e202301218.
[16] A. Marchuk, L. Neudert, O. Oeckler, W. Schnick, *Eur. J. Inorg. Chem.* **2014**, *2014*, 3427–3434.
[17] M. M. Pointner, O. Oeckler, W. Schnick, *Chem. Eur. J.* **2023**, e202301960.
[18] K. Nakamoto, *Infrared and Raman spectra of inorganic and coordination compounds, part B: applications in coordination, organometallic, and bioinorganic chemistry*, John Wiley & Sons, **2009**.
[19] V. A. Blatov, A. P. Shevchenko, D. M. Proserpio, *Cryst. Growth Des.* **2014**, *14*, 3576–3586.
[20] J. Smith, *Acta Crystallogr.* **1953**, *6*, 613–620.
[21] F. Karau, W. Schnick, *Z. Anorg. Allg. Chem.* **2006**, *632*, 231–237.
[22] S. Pennycook, *Annu. Rev. Mater. Sci.* **1992**, *22*, 171–195.
[23] K. Keller, E. Brendler, S. Schermler, C. Röder, G. Heide, J. Kortus, E. Kroke, *J. Phys. Chem. C* **2015**, *119*, 12581–12588.
[24] A. Marchuk, V. R. Celinski, J. Schmedt auf der Günne, W. Schnick, *Chem. Eur. J.* **2015**, *21*, 5836–5842.
[25] L. Neudert, F. Heinke, T. Bräuniger, F. J. Pucher, G. B. Vaughan, O. Oeckler, W. Schnick, *Chem. Commun.* **2017**, *53*, 2709–2712.
[26] R. D. Shannon, *Acta Crystallogr. Sect. A* **1976**, *32*, 751–767.
[27] S. Wendl, L. Eisenburger, M. Zipkat, D. Günther, J. P. Wright, P. J. Schmidt, O. Oeckler, W. Schnick, *Chem. Eur. J.* **2020**, *26*, 5010–5016.
[28] M.-H. Fang, C. O. M. Mariano, P.-Y. Chen, S.-F. Hu, R. S. Liu, *Chem. Mater.* **2020**, *32*, 1748–1759.
[29] R. Shafei, P. Strobel, P. J. Schmidt, D. Maganas, W. Schnick, F. Neese, *Phys. Chem. Chem. Phys.* **2024**, *26*, 6277–6291.
[30] E. O'Brannon III, Q. Williams, *Am. Mineral.* **2019**, *104*, 1656–1662.
[31] R. Suhrmann, K. Clusius, *Z. Anorg. Allg. Chem.* **1926**, *152*, 52–58.
[32] A. Stock, H. Grüneberg, *Ber. Dtsch. Chem. Ges.* **1907**, *40*, 2573–2578.
[33] D. Rubie, *Phase Transitions* **1999**, *68*, 431–451.
[34] H. Huppertz, *Z. Kristallogr. – Cryst. Mater.* **2004**, *219*, 330–338.
[35] D. Walker, *Am. Mineral.* **1991**, *76*, 1092–1100.
[36] D. Walker, M. Carpenter, C. Hitch, *Am. Mineral.* **1990**, *75*, 1020–1028.
[37] A. Coelho, TOPAS Academic version 6.1, Coelho Software, Brisbane (Australia), **2007**.
[38] H. M. Rietveld, *J. Appl. Crystallogr.* **1969**, *2*, 65–71.
[39] I. Gatan, DigitalMicrograph, version 3.6.5, Pleasanton (California, USA), **1999**.
[40] J. L. Lábár, *Ultramicroscopy* **2005**, *103*, 237–249.
[41] J. P. A. Stadelmann, jEMS software package, version 3.60907 U2011, Saas-Fee (Switzerland), **2008**.
[42] Thermo Fisher Scientific, Velox, version 2.14.0.703, Waltham (Massachusetts, USA), **2021**.
[43] Bruker-AXS, APEX3, version 2016.5-0, Karlsruhe (Germany), **2001**.
[44] O. D. Rigaku, CrysAlis^{Pro}, version 171.42.102a, Yarnton, Oxfordshire (England), **2017**.
[45] G. M. Sheldrick, *SADABS, v.2: Multi-Scan Absorption Correction*; Bruker-AXS, Billerica, MA, **2012**.
[46] G. M. Sheldrick, *Acta Crystallogr. Sect. A* **2018**, *71*, 112–122.
[47] K. Brandenburg, Diamond, version 3.2k, Bonn (Germany), **1997–2014**.
[48] A. S. Wills, VaList – A bond valence calculation and analysis program, version 4.0.7, University College London, London (England), **1998–2010**.
[49] N. E. Brese, M. O'Keeffe, *Acta Crystallogr. Sect. B* **1991**, *47*, 192–197.
[50] K. Momma, F. Izumi, *J. Appl. Crystallogr.* **2011**, *44*, 1272–1276.
[51] R. Hoppe, *Angew. Chem.* **1970**, *82*, 7–16; *Angew. Chem. Int. Ed.* **1970**, *9*, 25–34.
[52] R. Hoppe, *Angew. Chem.* **1966**, *78*, 52–63; *Angew. Chem. Int. Ed.* **1966**, *5*, 95–106.
[53] K. Landskron, PhD thesis, Ludwig-Maximilians-Universität (Germany), **2001**.
[54] P. Pust, A. S. Wochnik, E. Baumann, P. J. Schmidt, D. Wiechert, C. Scheu, W. Schnick, *Chem. Mater.* **2014**, *26*, 3544–3549.
[55] M. Ludwig, R. Niewa, R. Kniep, *Z. Naturforsch. B* **1999**, *54*, 461–465.
[56] C. Hecht, F. Stadler, P. J. Schmidt, J. r. S. auf der Günne, V. Baumann, W. Schnick, *Chem. Mater.* **2009**, *21*, 1595–1601.
[57] J. A. Kechele, O. Oeckler, F. Stadler, W. Schnick, *Solid State Sci.* **2009**, *11*, 537–543.
[58] K. Horky, W. Schnick, *Eur. J. Inorg. Chem.* **2017**, *2017*, 1100–1106.
[59] T. Schlieper, W. Milius, W. Schnick, *Z. Anorg. Allg. Chem.* **1995**, *621*, 1380–1384.
[60] P. Strobel, R. Niklaus, P. J. Schmidt, W. Schnick, *Chem. Eur. J.* **2018**, *24*, 12678–12685.

Manuscript received: February 24, 2024
Accepted manuscript online: March 14, 2024
Version of record online: April 4, 2024